

AI-Powered Pressure Reconstruction and Parameter Inversion for Carbonate Reservoirs: A Physics-Guided Deep Learning Approach[#]

Ruofan Yan ^{1,2*}, Jing Wang ^{1,2}, Huiqing Liu ^{1,2}

1. National Key Laboratory of Petroleum Resources and Engineering in China University of Petroleum, Beijing 102249, China

2. MOE Key Laboratory of Petroleum Engineering in China University of Petroleum, Beijing 102249, China

(*Corresponding Author: roven233@163.com)

ABSTRACT

Dynamic analysis and reserve estimation for deep fractured-vuggy carbonate reservoirs pose significant challenges due to severe reservoir heterogeneity, complex production dynamics, and the extreme scarcity of key static formation pressure data. While conventional physics-based models struggle with such data sparsity, standard Artificial Intelligence methods often lack the physical consistency and interpretability required for high-stakes engineering applications. To bridge this gap, this paper introduces PG-TCRN, an innovative physics-guided AI architecture that integrates a Temporal Convolutional Network with a Long Short-Term Memory network to synergize deep learning with domain knowledge. Guided by a composite physics-based loss function, this model leverages continuous production data to intelligently reconstruct a reliable formation pressure profile from only a few static measurements. Subsequently, with the material balance equation serving as a strong physical constraint, our framework transforms the history matching task into a low-dimensional optimization problem, enabling the accurate inversion of key parameters like dynamic reserves and water influx coefficient. Application to a real-world case from the Z Reservoir validates our approach, achieving a precise match of the production history and confirming the physical reliability of the inverted parameters. Furthermore, the framework's interpretable results quantify the contribution of different energy sources, revealing the dominant reservoir drive mechanism. This study presents an efficient and interpretable new paradigm for AI-driven dynamic analysis in fractured-vuggy reservoirs, offering a powerful tool for data-scarce scenarios.

Keywords: artificial intelligence, physics-guided deep learning, fractured-vuggy reservoirs, dynamic parameter inversion, intelligent energy systems, material balance equation

NONMENCLATURE

Abbreviations

MBE	Material Balance Equation
TCN	Temporal Convolutional Network
LSTM	Long Short-Term Memory
RNN	Recurrent Neural Network
MSE	Mean Square Error
MAPE	Mean Absolute Percentage Error
TV	Total Variation

Symbols

N	Dynamic oil in place
$N_p(t)$	Cumulative oil
$W_p(t)$	Cumulative water
$p(t)$	Reservoir pressure
p_i	Initial reservoir pressure
$B_o(p)$	Oil FVF
B_{oi}	Initial oil FVF
B_w	Water FVF
α	Water-influx coefficient
$W_e(t)$	Water influx term
C_w	Water compressibility
C_f	Rock compressibility
S_{wi}	Initial water saturation
LHS(t)	MBE left-hand side
RHS(t)	MBE right-hand side
$r(t)$	MBE residual
T	Sequence length
F	Feature dimension
ν_c	Cut-off frequency
L	Low-pass kernel span
ω_t	Time weight

1. INTRODUCTION

Deep fractured-vuggy carbonate reservoirs represent a vital component of global oil and gas resources. They hold particular strategic and economic significance in regions such as China's Tarim Basin, where proven reserves are immense^[1,2]. These reservoirs are

[#] This is a paper for the 17th International Conference on Applied Energy - ICAE2025, Dec. 8-12, 2025, Bangkok, Thailand.

typically characterized by deep burial, severe reservoir heterogeneity, and complex, unpredictable production dynamics^[3,4]. These characteristics present two primary challenges for dynamic analysis and reserve estimation. First, while conventional methods like material balance and numerical simulation are built on clear physical principles, they are prone to non-uniqueness and sensitivity to initial values when applied to inverse problems with sparse monitoring data^[5-7]. Second, although deep neural networks possess strong non-linear fitting capabilities for production time-series, their lack of verifiable physical consistency and interpretability hinders their application in practical engineering decision-making^[8,9].

For deep fractured-vuggy carbonate reservoirs, continuous downhole pressure monitoring is often infeasible due to prohibitive costs and technical risks. While static gradient tests provide crucial static reservoir pressure data, they are disruptive to normal well production, resulting in only sporadic and extremely sparse pressure measurements being available^[10,11]. In this context, material balance methods like the Havlena–Odeh straight-line analysis remain common in low-data-density scenarios, but their validity depends on a series of idealized assumptions and a sufficient amount of stable pressure data^[5]. Therefore, the essence of the current problem is to achieve robust history matching and inversion of dynamic parameters under the stringent constraints of sparse data combined with strong physical laws.

In recent years, various techniques have been widely applied to history matching, including deterministic optimization based on sensitivity or adjoint methods, stochastic assimilation using ensemble Kalman filters or smoothers, and frameworks for re-parameterization and uncertainty quantification of high-dimensional parameter fields^[6,7]. However, when available pressure observations are extremely sparse, these methods also face challenges related to insufficient information, reliance on regularization, and a lack of convergence robustness. Concurrently, data-driven methods have advanced rapidly in modeling time-series for energy and process control systems. Research in deep time-series modeling shows that modern architectures can achieve higher prediction stability and interpretability even with missing data points, non-uniform sampling, and multivariate coupling. For instance, the deep Koopman model enhances the robustness of long-term predictions by learning an approximate linear manifold^[12], while Transformer-based models with attention mechanisms have demonstrated strong long-term memory and

feature selection capabilities in applications like wind power and load forecasting^[13-15].

To bridge the gap between physical models and data-driven approaches, technologies such as Physics-Informed Neural Networks (PINNs) and Physics-Guided Machine Learning (PIML) have emerged. These methods embed physical constraints like conservation laws, monotonicity, and boundary conditions into the loss function or network architecture to guide the learning of physically self-consistent solutions, particularly in small-sample and extrapolation scenarios^[16,17]. For example, a physics-guided, non-iterative optimal control framework has proven the effectiveness of PIML in geothermal reservoir optimization and building control systems^[18], while PINNs driven by structural or trend priors have significantly improved extrapolation stability and interpretability in chiller optimal control and energy consumption modeling^[19]. These advancements inspire a new approach for deep fractured-vuggy reservoirs with sparse pressure constraints: first, reconstruct a continuous pressure profile using physical priors, and then perform parameter inversion constrained by reservoir engineering principles to obtain key water influx parameters. However, for the inverse problem studied in this paper—which involves coupled unknown functions and unknown global parameters—designing a single, end-to-end PINN or PIML framework still presents significant optimization challenges.

To overcome this dilemma, this paper proposes an innovative physics-guided decoupled framework that decomposes the ill-posed problem into two sequential sub-tasks: (1) Physics-guided pressure reconstruction: A bespoke hybrid time-series network (PG-TCRN) is utilized, taking continuous production data as input. Guided by a composite loss function that embeds multiple physical priors such as smoothness, monotonicity, and boundary conditions, this stage generates a high-quality, continuous pressure profile from sparse static pressure measurements. (2) Physics-constrained parameter inversion: The reconstructed, complete pressure sequence is treated as a known input. With the material balance equation serving as a strong physical constraint, the problem is transformed into a well-defined, low-dimensional optimization task to accurately invert key water influx parameters.

This work focuses on three primary contributions: (1) It proposes a physics-guided decoupled workflow tailored for extremely sparse pressure scenarios, explicitly separating reconstruction and inversion to mitigate the ill-posed nature of the problem. (2) It develops the PG-TCRN (Physics-Guided Temporal Convolution–Recurrent Network) and employs a

composite physical loss to ensure the smoothness and physical plausibility of the reconstructed curve. (3) It validates the framework on a real-world oilfield case, demonstrating accurate history matching over the well's life cycle. This research offers a efficient and interpretable new paradigm for reservoir history matching and dynamic parameter inversion from sparse dynamic data.

2. PROBLEM DEFINITION AND EQUATIONS

During the primary recovery of deep, bottom-water drive, fractured-vuggy reservoirs, the expansion of connate water within the vugs and the energy released from reservoir rock deformation are particularly significant due to the high overburden pressure. Assuming the conservation of oil and water volumes, the MBE for a bottom-water drive, fractured-vuggy reservoir is expressed as:

$$\begin{aligned} N_p(t)B_o(\hat{p}(t)) &= N[B_o(\hat{p}(t)) - B_{oi}] \\ &+ W_e(t) - W_p(t)B_w \\ &+ NB_{oi} \frac{C_w S_{wi} + C_f}{1 - S_{wi}} [p_i - \hat{p}(t)] \end{aligned} \quad (1)$$

In this equation, the left-hand side represents the subsurface volume of cumulative oil production. The terms on the right-hand side are, respectively: first, the volume change due to the expansion of the oil phase as reservoir pressure declines; second, the volume of water influx from the bottom aquifer into the reservoir; third, the subsurface volume of cumulative water production; and fourth, the volume change attributed to the compressibility of the vugs and the connate water.

To achieve closure for the system of equations and reduce the degrees of freedom, a parameterized model for the water influx term is required, which transforms the problem into one of estimating a finite set of parameters. In this study, water influx is treated as a response to the pressure drop and is represented by a linear approximation:

$$W_e(t) = \alpha \cdot N \cdot [p_i - \hat{p}(t)] \quad (2)$$

Where α is the water influx coefficient (MPa^{-1}), characterizing the strength of the aquifer response per unit of pressure drop.

Substituting Eq. (2) back into Eq. (1) yields a balance equation with only two unknown parameters:

$$\begin{aligned} N_p(t)B_o(\hat{p}(t)) &= N[B_o(\hat{p}(t)) - B_{oi}] + \alpha N[p_i - \hat{p}(t)] \\ &- W_p(t)B_w + NB_{oi} \frac{C_w S_{wi} + C_f}{1 - S_{wi}} [p_i - \hat{p}(t)] \end{aligned} \quad (3)$$

To clearly formulate the optimization objective, we first define the right-hand side of Equation (3) as a parameterized function, denoted by Φ :

$$\begin{aligned} \Phi(t; \hat{p}(t), N, \alpha) &= N[B_o(\hat{p}) - B_{oi}] + \alpha N \Delta p \\ &- W_p B_w + NB_{oi} \frac{C_w S_{wi} + C_f}{1 - S_{wi}} \Delta p \end{aligned} \quad (4)$$

This allows the MBE to be simplified into the compact form of Equation (5):

$$N_p(t)B_o(\hat{p}(t)) = \Phi(t; \hat{p}(t), N, \alpha) \quad (5)$$

In the above relationship, the oil formation volume factor B_o , is a function of the formation pressure. Acquiring direct pressure measurements through methods like static pressure surveys is often disruptive to normal production operations, resulting in a sparse set of available data points. For this reason, we employ a neural network model to reconstruct a continuous time series of the average formation pressure.

Given the availability of the continuous formation pressure $\hat{p}(t)$ and the corresponding B_o values, the parameter inversion problem is explicitly defined as follows: conditioned on the production history and the reconstructed pressure trajectory, solve for the optimal set of parameters (N, α). The optimization objective is to minimize the material balance residual, $r(t)$, at every time step:

$$r(t) = N_p(t)B_o(\hat{p}(t)) - \Phi(t; \hat{p}(t), N, \alpha) \quad (6)$$

Collectively, Equations (1) through (6) establish the physically-constrained foundation for the parameter inversion stage of this study.

3. METHODOLOGY

To address the ill-posed inversion of reservoir parameters from sparse pressure observations, this study proposes an innovative, two-stage physics-guided framework. The core strategy is to decouple the complex problem into two sequential sub-tasks. First, a hybrid deep learning model, the Physics-Guided Temporal Convolutional-Recurrent Network (PG-TCRN), is utilized. This TCN-LSTM network is trained with a composite loss function embedding physical priors—such as smoothness and boundary conditions—to reconstruct a continuous and plausible average pressure profile from production dynamics and scarce static measurements. Subsequently, this high-quality pressure sequence transforms the inverse problem into a well-posed, low-dimensional optimization task. With the material balance equation serving as a hard constraint, key parameters, including dynamic reserves and the water influx coefficient, are accurately inverted by minimizing the physical residual.

3.1 Physics-guided continuous pressure reconstruction

Given the sparsity of static pressure measurements, it is imperative to first obtain a continuous and physically plausible average formation pressure curve. If the pressure curve contains non-physical high-frequency oscillations or spikes, the associated errors will propagate directly into the material balance equation through the pressure-drop term, thereby amplifying the systematic bias in the MBE residual. Therefore, the pressure reconstruction must simultaneously satisfy the dual requirements of fitting the static pressure measurements and adhering to morphological

constraints. This process must be implemented in an end-to-end differentiable manner, allowing the shape priors to be incorporated into backpropagation.

The model input is defined as the production dynamics feature matrix $X \in R^{T \times F}$, where T is the time length and F is the feature dimension. We construct a hybrid model architecture named PG-TCRN (Physics-Guided Temporal Convolutional-Recurrent Network), which combines a Temporal Convolutional Network (TCN) with a Long Short-Term Memory (LSTM) network. The model architecture is illustrated in the figure 1.

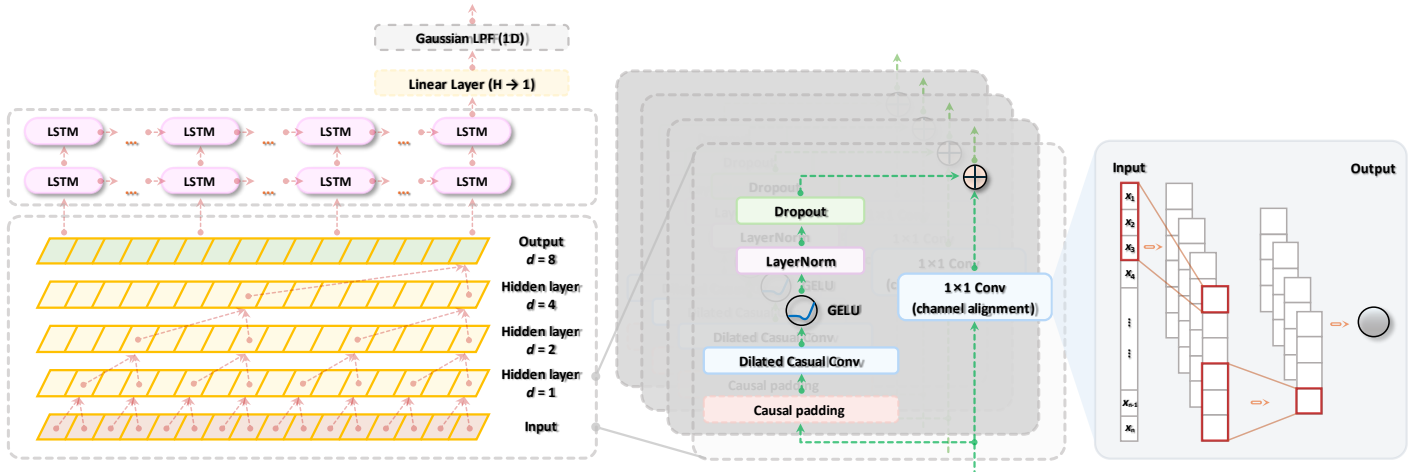


Fig. 1 Physics-guided temporal convolutional-recurrent network (PG-TCRN) architecture

First, a one-dimensional Temporal Convolutional Network (TCN) module is employed as a feature extractor. Through the use of causal and dilated convolutions, it produces the following output:

$$H^{tcn} = \Phi_{TCN}(X) \in R^{T \times C} \quad (7)$$

Subsequently, the deep feature sequence, H^{tcn} , extracted by the TCN is fed into a two-layer Long Short-Term Memory (LSTM) network to model medium- to long-term dependencies, yielding:

$$H^{lstm} = \Psi_{LSTM}(H^{tcn}) \in R^{T \times H}, \quad (8)$$

$$z(t) = W_{in} H^{lstm}(t) + b_{lin}$$

As a classic recurrent neural network, the core advantage of an LSTM lies in its gating mechanism, which effectively addresses the vanishing and exploding gradient problems inherent in traditional RNNs. This enables the network to learn and retain long-term dependencies within time-series data. A diagram of the LSTM unit is shown below.

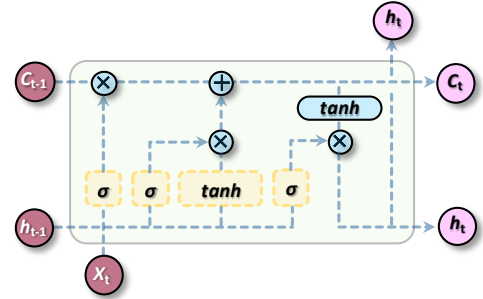


Fig. 2 Basic structure of LSTM cell

Stacked LSTMs, as deep neural networks with multiple hidden layers, have become an established technique for solving complex sequence prediction problems^[20]. The architecture of a stacked LSTM is illustrated in Figure 3. This network consists of two LSTM layers, each containing multiple interconnected LSTM units. The first LSTM layer receives the raw data as input, while the input for any subsequent LSTM layer is the hidden state from the preceding layer. Therefore, in contrast to a standard LSTM, the hidden state of a given layer in a stacked LSTM propagates both through time to the next time step and is also passed to the next layer.

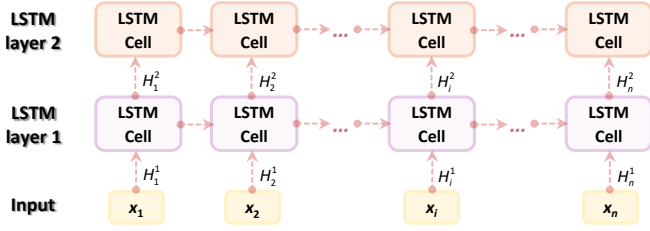


Fig. 3 The architecture of stacked LSTM

Subsequently, a linear layer maps the hidden states to a preliminary pressure trajectory. However, pressure profiles generated directly by the neural network may exhibit physically implausible, high-frequency local oscillations. In a complex, multi-porosity medium such as a fractured-vuggy reservoir, the dynamic evolution of the average formation pressure is governed by the fundamental principles of fluid dynamics. The propagation of a pressure transient through the porous medium, induced by fluid movement during production, is fundamentally a diffusion process. The governing diffusion equation dictates that any pressure wave is rapidly attenuated and smoothed with distance and time as it propagates^[21,22]. From the principle of material balance, the rate of pressure change is given by:

$$\frac{dp}{dt} \propto -\frac{qB}{\phi V_p c_t} \quad (9)$$

For a given production rate q , the vast pore volume, ϕV_p and low total compressibility, c_t , characteristic of these reservoirs constrain the rate of pressure decline. This results in a macroscopically smooth and slow-varying pressure response. Therefore, to ensure our model honors this physical behavior, we incorporate the "smooth and gradual change" as a physical prior in the training process. This is achieved by introducing a symmetric, differentiable Gaussian low-pass filter at the output, which implements smoothing via discrete convolution:

$$\hat{p}(t) = \sum_{\tau=-L}^L g_\sigma(\tau) z(t-\tau), \quad (10)$$

$$g_\sigma(\tau) = \frac{e^{-\tau^2/(2\sigma^2)}}{\sum_{k=-L}^L e^{-k^2/(2\sigma^2)}}$$

The kernel radius L and scale σ determine the effective support and the strength of the smoothing. This low-pass head is implemented as a small convolutional layer, acting analogously to a signal processing filter. It smooths the output curve to ensure that the reconstructed average formation pressure sequence is consistent with the characteristics of fluid pressure propagation in fractured-vuggy media.

To guide the model's training towards a physically consistent solution, we designed a composite loss

function whose objective comprises four components: anchor point fidelity, shape regularization, a frequency-domain constraint, and an initial boundary condition. Let the set of sparse pressure measurement time steps be $\mathcal{S} \subset \{1, \dots, T\}$, the observed pressure values be p_k^* , the first-order difference be $\Delta \hat{p}(t) = \hat{p}(t) - \hat{p}(t-1)$ and the second difference as $\Delta^2 \hat{p}(t) = \hat{p}(t+1) - 2\hat{p}(t) + \hat{p}(t-1)$. The total loss is then formulated as:

$$\begin{aligned} \mathcal{L}_{\text{press}} = & \frac{1}{|\mathcal{S}|} \sum_{k \in \mathcal{S}} (\hat{p}_k - p_k^*)^2 \\ & + \lambda_{\text{curv}}^{\text{eff}} \frac{1}{T-2} \sum_{t=2}^{T-1} \rho_\delta(\Delta^2 \hat{p}(t)) + \lambda_{\text{tv}} \frac{1}{T-1} \sum_{t=2}^T |\Delta \hat{p}(t)| \quad (11) \\ & + \lambda_{\text{spec}} \frac{\sum_{v \geq v_c} |\mathcal{F}\{\hat{p}\}(v)|^2}{\sum_v |\mathcal{F}\{\hat{p}\}(v)|^2} + \lambda_{\text{anchor}} (\hat{p}_1 - p_i)^2 \end{aligned}$$

The first term, anchor point fidelity, ensures that the reconstructed curve honors all sparse, measured static pressure points.

The second term provides shape regularization to maintain the overall smoothness of the curve. It consists of two components: a penalty on the first-order difference, $\Delta \hat{p}(t)$, to constrain the total variation of the curve, and a penalty on the second-order difference, $\Delta^2 \hat{p}(t)$, to suppress high curvature. The penalty on the second-order difference employs the Huber loss, which is more robust than the standard L_2 loss, allowing it to suppress "ringing" artifacts while preserving gradual changes in curvature:

$$\rho_\delta(u) = \begin{cases} \frac{1}{2} u^2, & |u| < \delta \\ \delta \left(|u| - \frac{1}{2} \delta \right), & \text{otherwise} \end{cases} \quad (12)$$

To encourage the model to prioritize fitting the data points during the initial training phase, the smoothing weight $\lambda_{\text{curv}}^{\text{eff}}$ is dynamically adjusted according to the training progress $\phi \in [0, 1]$ using a linear annealing schedule:

$$\lambda_{\text{curv}}^{\text{eff}} = \lambda_{\text{curv}} (1.2 - 0.8\phi) \quad (13)$$

The third term is a frequency-domain constraint. Complementing the shape regularization, this term directly penalizes non-physical, high-frequency components above a specified cutoff frequency v_c . The cutoff frequency v_c and the low-pass filter scale σ are determined by minimizing a validation metric via a grid search.

The final term is the initial boundary condition, which constrains the starting point of the trajectory, \hat{p}_1 ,

to be consistent with the known initial formation pressure, p_i .

By minimizing this composite loss function, the PG-TCRN network generates a pressure trajectory that is both faithful to the observational data and consistent with physical principles, thus providing a stable and reliable input for subsequent material balance calculations.

3.2 Parameter Inversion under Material Balance Constraints

Building upon the continuous average formation pressure sequence $\hat{p}(t)$ obtained previously, this section leverages the material balance equation as a strong physical constraint to jointly invert for the dynamic reserves (N) and the water influx strength parameter (α) using an optimization algorithm. With the pressure trajectory $\hat{p}(t)$ serving as a prior input, the history matching task is formulated as an optimization problem aimed at minimizing an objective function. This function is defined as the mean squared error (MSE) of the material balance residual, $r(t)$, across the entire production history. This approach assigns equal weight to all time steps, seeking an optimal set of parameters (N, α) by minimizing the global residual:

$$L_J = \frac{1}{T} \sum_{t=1}^T r(t)^2 \quad (14)$$

To ensure the inverted parameters N and α remain within their physically feasible domain, we employ a differentiable reparameterization technique. Instead of directly optimizing the parameters, we optimize their unconstrained counterparts in the logarithmic domain and map them back to the original space via an exponential transformation:

$$N = \exp(\hat{N}), \quad \alpha = \exp(\hat{\alpha}) \quad (15)$$

Here, \hat{N} and $\hat{\alpha}$ are unconstrained latent variables within the optimization process. Furthermore, to enhance the stability of the optimization and prevent the parameters from drifting in intervals dominated by noise, a lightweight L2 regularization term is incorporated into the objective function:

$$L_{\text{reg}} = \lambda_N (\hat{N} - \hat{N}_{\text{prior}})^2 + \lambda_\alpha (\hat{\alpha} - \hat{\alpha}_{\text{prior}})^2 \quad (16)$$

The final objective function is therefore the sum of the MSE and regularization terms:

$$L_{\text{total}} = L_J + L_{\text{reg}} \quad (17)$$

This optimization problem is solved using a first-order, gradient-based method, complemented by a learning rate scheduler and an early stopping criterion. To mitigate numerical issues arising from the different

scales of various physical quantities, all input variables are normalized before being passed to the loss function.

4. CASE STUDY

4.1 Dataset and Experimental Setup

4.1.1 Data source and features

To validate the effectiveness and practicality of the proposed framework, we conduct a case study using dynamic data from a real production well in the Z oilfield, located in China's Tarim Basin. This deep, fractured-vuggy carbonate reservoir is characterized by extreme heterogeneity and complex production dynamics. Harsh downhole conditions make continuous pressure monitoring prohibitively expensive, resulting in exceptionally sparse data, which provides an ideal and challenging test case for our method.

The dataset contains the well's complete daily production history, including cumulative oil (N_p) and water (W_p) production, alongside other dynamic features. Critically, only six discrete static pressure measurements were available over the well's entire production life.

4.1.2 Physical parameter setup

The rock and fluid properties required for the material balance equation were determined based on the geological and PVT analyses of the reservoir block. Some of these are known constants, while others are typical values established from offset well data and empirical knowledge, as detailed in table. 1:

Table. 1 Reservoir and fluid properties

Parameter	Value	Unit
p_i	85.2	MPa
B_{oi}	2.463	
B_w	1.034	
C_w	4.5×10^{-4}	MPa ⁻¹
C_f	1.0×10^{-4}	MPa ⁻¹
S_{wi}	10	%

4.1.3 Model implementation and setup

The algorithmic framework for this research was implemented using *PyTorch* and adheres to the two-stage process outlined in the Methodology section.

Stage One: The PG-TCRN model, with 3 ConvTCN and 2 LSTM modules (hidden dimension: 64), was trained using an Adam optimizer (initial LR: 1E-3). Weights for the composite loss function were determined via cross-validation to balance data fidelity with physical regularization.

Stage Two: Using the reconstructed pressure profile, the physical residual loss was minimized with the Adam

optimizer to solve for dynamic reserves (N) and the water influx coefficient (α). This optimization typically converged within several hundred iterations.

These settings ensure the objectivity and reproducibility of the entire case study process.

4.2 Results and Analysis

4.2.1 Validation of pressure reconstruction performance

The pressure curve reconstructed by the PG-TCRN model is presented in Figure 4.

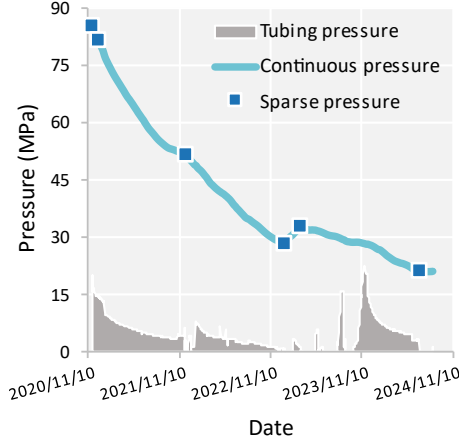


Fig. 4 PG-TCRN: Pressure Reconstruction Results

It is visually apparent that the reconstructed curve not only passes precisely through all known data anchor points but also demonstrates a high degree of fidelity to the measured static pressure points.

In contrast to the highly fluctuating tubing pressure curve that served as an input reference, the model produced a continuous and smooth formation pressure curve, successfully extracting a more stable and realistic underlying pressure dynamic from the noisy signal.

To quantitatively assess the physical plausibility of the reconstructed curve, Table 2 summarizes its morphology and boundary-consistency metrics. The High Freq Ratio is only 0.038%, indicating that the energy in the frequency domain above the cutoff frequency, ν_c , is negligible. Combined with the Total Variation (TV) and curvature energy values, it is evident that the curve has no significant "sawtooth" or "ringing" artifacts at either the first- or second-order levels. Furthermore, the initial anchor point error is merely 0.38% of the original formation pressure, which confirms the baseline consistency in magnitude. Collectively, these metrics verify that the physics-guided mechanism successfully integrated engineering priors into the neural network's training process. Therefore, using the reconstructed pressure, $\hat{p}(t)$, as the input for Equations (1)–(3) is both physically acceptable and stable.

Table. 2 Quantitative metrics for pressure reconstruction quality

Metric	Value	Description
TV	86.94	Metric of 1st-order smoothness; suppresses sawtooth artifacts.
Curvature Energy	5.047	Metric of 2nd-order smoothness; suppresses ringing artifacts.
High Freq Ratio	3.82×10^{-4}	Ratio of power above the cutoff frequency to measure non-physical oscillations.
Anchor Error	0.326	Absolute error (MPa) of the initial pressure prediction, ensuring baseline consistency.

4.2.2 Parameter Inversion and History Matching

Upon obtaining the high-quality, continuous pressure curve, the process proceeds to the inversion stage for key physical parameters related to water influx. With the pressure profile, $\hat{p}(t)$, held constant, the parameters for dynamic reserves and water influx strength are estimated by minimizing the robust weighted loss of the material balance equation's residual at each time step. The results are presented in table 3:

Table. 3 Inverted parameters and goodness of fit

Metric	Value	Unit
N	12.61	10^4m^3
α	6.36×10^{-3}	MPa^{-1}
MBE_RMSE	909.29	m^3
N_p _MAPE	0.218	%

The ultimate validation of the history match lies in the model's ability to reproduce the historical production dynamics using the inverted parameters. First, the two sides of the material balance equation are compared in the MBE space. Let:

$$LHS = N_p B_o \quad (18)$$

$$RHS = N[B_o - B_{oi}] + W_e - W_p B_w + NB_{oi} \frac{C_w S_{wi} + C_f}{1 - S_{wi}} [p_i - \hat{p}] \quad (19)$$

A comparison plot of the LHS versus the RHS is generated to verify historical consistency.

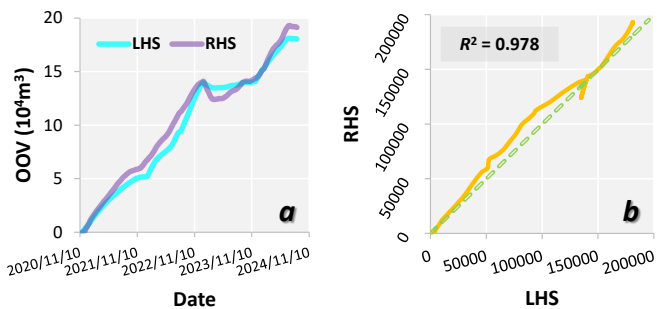


Fig. 5 Verification of material balance closure: temporal comparison and diagonal cross-plot analysis: (a) Temporal comparison of LHS and RHS; (b) RHS vs. LHS diagonal cross-plot verification

The cumulative oil production, calculated using the inverted parameters (N , α) via the material balance equation, was compared against the actual historical cumulative production. As seen in figure 5, the two curves show a high degree of overlap throughout the entire production history, indicating that the method achieves a precise fit of the historical production dynamics and confirms that the conservation relationship holds true for the inverted parameters.

To further investigate the drive mechanisms of the fractured-vuggy reservoir, the RHS is decomposed into four key components: the oil expansion term, the water influx term, the water production term, and the total compressibility term.

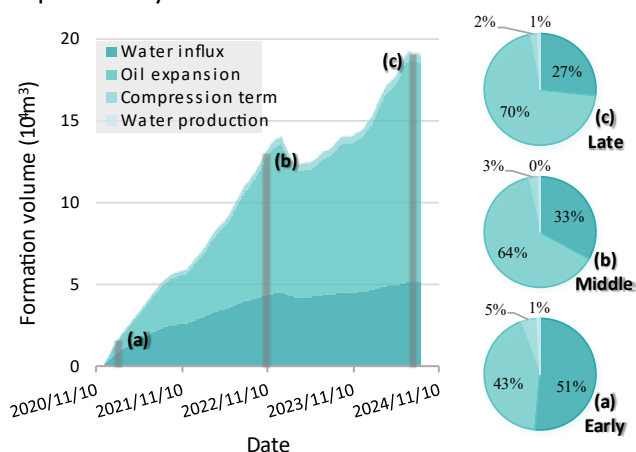


Fig. 6 RHS components and stage shares

The analysis clearly indicates that during the early production stage, the decline in formation pressure is gradual. Nevertheless, water influx activates before a significant pressure differential is established and rapidly becomes the dominant drive mechanism. This suggests the reservoir is connected to a highly active edge or bottom aquifer that provides immediate pressure support. As production continues, the pressure differential across the reservoir grows, leading to a progressively larger contribution from the expansion of

the reservoir fluids. By the later stages of production, fluid expansion has supplanted water influx as the primary drive mechanism. This sequence reveals the transition of the dominant drive mechanisms at different production phases of the reservoir.

5. CONCLUSION

Dynamic analysis of deep fractured-vuggy carbonate reservoirs presents significant challenges due to sparse formation pressure data, which creates a dilemma for engineers. Traditional physical models often lack adaptability, while purely data-driven methods lack physical constraints. To address this issue, we have innovatively proposed and validated a physics-guided hybrid framework. The main conclusions of this study are as follows:

(1) This research introduces an innovative, decoupled two-stage framework that has been proven to be an effective strategy for solving such complex engineering inverse problems. By strategically decomposing the problem into two logically sequential sub-tasks—"physics-guided pressure reconstruction" and "physics-constrained parameter inversion"—the framework significantly reduces the difficulty of the solution process and successfully integrates the powerful non-linear mapping capabilities of neural networks with the physical prior knowledge of reservoir engineering.

(2) The designed physics-guided temporal convolutional-recurrent network (PG-TCRN) successfully reconstructed a continuous, smooth, and physically plausible average static formation pressure curve under the strong constraint of only 6 sparse observation points. Experiments demonstrate that through shape regularization and frequency-domain suppression, physical prior knowledge can be transformed into learnable mathematical constraints, yielding a continuous, stable, and engineering-credible pressure curve that provides a stable input for the subsequent inversion stage.

(3) In its application to a real-world oilfield case, the framework, using the reconstructed pressure curve, accurately matched the entire production history of the well's current life cycle through the subsequent material balance inversion.

In summary, this paper provides a robust, efficient, and interpretable new paradigm for history matching and the inversion of key water influx parameters for fractured-vuggy reservoirs using sparse dynamic data. The framework not only offers technical support for the dynamic analysis of deep fractured-vuggy carbonate reservoirs, such as the A oilfield, but may also serve as a

valuable reference for other engineering domains facing similar challenges of data scarcity.

ACKNOWLEDGEMENT

This work was supported by National Natural Science Foundation of China (No. 52074316).

REFERENCE

- [1] C. Jia and M. Zheng and Yongfeng Zhang Unconventional hydrocarbon resources in China and the prospect of exploration and development, 2012, 39.
- [2] Tian, J., Yang, H., Zhu, Y., et al. Geological conditions for hydrocarbon accumulation and key technologies for exploration and development in Fuman Oilfield, Tarim Basin. *Acta Petrolei Sinica*, 2021, 42(8), 971-985.
- [3] Jiao, F.; et al. Practice and knowledge of volumetric development of deep fractured-vuggy carbonate reservoirs in Tarim Basin, NW China. *Petroleum Exploration and Development*, 2019, 46(3): 576–589.
- [4] Ma, Y.; et al. Review on exploration and development of Shunbei ultra-deep carbonate oil & gas field, Tarim Basin. *Petroleum Exploration and Development*, 2022, 49(1): 1–16.
- [5] Havlena, D.; Odeh, A.S. The Material Balance as an Equation of a Straight Line. *Journal of Petroleum Technology*, 1963, 15(8): 896–900.
- [6] Oliver, D.S.; Reynolds, A.C.; Liu, N. Recent progress on reservoir history matching: A review. *Computational Geosciences*, 2011, 15: 185–221.
- [7] Emerick, A.A.; Reynolds, A.C. History matching time-lapse seismic data using the ensemble Kalman filter with multiple data assimilations. *Computational Geosciences*, 2012, 16: 639–659.
- [8] van Zyl, C.; Ye, X.; Naidoo, R. Harnessing explainable AI for feature selection in time-series energy forecasting: A comparative analysis of Grad-CAM and SHAP. *Applied Energy*, 2024, 353: 122079.
- [9] Hu, Y.; et al. Temporal collaborative attention for wind power forecasting (TCOAT). *Applied Energy*, 2024, 357: 122502.
- [10] Reliability Analysis of Permanent Downhole Monitoring Systems. *SPE Drilling & Completion*, 2001, 16(1): 60–67.
- [11] de Souza, M.J.M.; et al. Reliability of permanent downhole systems: Minimum sample and quality index. *Petroleum Research*, 2024.
- [12] Ding, J.; et al. From irregular to continuous: The deep Koopman model for time series forecasting of energy equipment. *Applied Energy*, 2024, 364: 23138.
- [13] Lim, B.; Arik, S.O.; Loeff, N.; Pfister, T. Temporal Fusion Transformers for interpretable multi-horizon time-series forecasting. *International Journal of Forecasting*, 2021, 37(4): 1748–1764.
- [14] Liu, L.; et al. Interpretable feature-temporal transformer for short-term wind power forecasting. *Applied Energy*, 2024, 374: 1214181.
- [15] Kim, H.J.; Kim, M.K. A novel deep learning-based forecasting model optimized by heuristic algorithm for energy management of microgrid. *Applied Energy*, 2023, 332: 120525.
- [16] Raissi, M.; Perdikaris, P.; Karniadakis, G.E. Physics-informed neural networks: A deep learning framework for solving forward and inverse problems involving nonlinear partial differential equations. *Journal of Computational Physics*, 2019, 378: 686–707.
- [17] Ma, Z.; et al. A review of physics-informed machine learning for building energy systems. *Applied Energy*, 2025, 381: 1225534.
- [18] Yan, B.; et al. Physics-informed machine learning for noniterative optimization in geothermal energy recovery. *Applied Energy*, 2024, 365: 123179.
- [19] Liang, X.; et al. Physics-informed neural network for chiller plant optimal control with structure-type and trend-type prior knowledge. *Applied Energy*, 2025, 390: 125857.
- [20] Brownlee J. Long short-term memory networks with python: develop sequence prediction models with deep learning[M]. *Machine Learning Mastery*, 2017.
- [21] J. Bear Dynamics of Fluids in Porous Media, 1975: 120.
- [22] A. V. Everdingen and W. Hurst The Application of the Laplace Transformation to Flow Problems in Reservoirs, 1949: 1.